Electronic Supplementary Information for

A Microporous **shp**-Topology Metal–Organic Framework with an Unprecedented High-Nuclearity Co_{10}-Cluster for Iodine Capture and Histidine Detection

Kun Wu,[a] Yong-Liang Huang,[b] Ji Zheng,[a] Dong Luo,[a] Mo Xie,[a] Yan Yan Li,[a] Weigang Lu*[a] and Dan Li*[a]

[a]College of Chemistry and Materials Science, and Guangdong Provincial Key Laboratory of Functional Supramolecular Coordination Materials and Applications, Jinan University, Guangzhou 510632, P. R. China E-mail: weiganglu@jnu.edu.cn; danli@jnu.edu.cn
[b]Department of Chemistry, Shantou University Medical College, Shantou 515041, P. R. China

Contents

Section 1. Synthesis of JNU-201 and JNU-202

Synthesis of JNU-201

A mixture of $Co(NO_3)_2 \cdot 6H_2O$ (14.8 mg, 0.051 mmol), H_4BTTB (13.6 mg, 0.024 mmol), N,N-dimethylformamide (DMF, 2.0 mL), EtOH (1.0 mL), H_2O (1.0 mL), CF_3COOH (4 μL) and 4 mg imidazole was placed in a 10 mL glass vial and heated at 90 °C for 72 h. After it was cooled to room temperature at a rate of 5 °C h^{-1}, the pink block crystals were collected.

Synthesis of JNU-202

A mixture of $Co(NO_3)_2 \cdot 6H_2O$ (14.8 mg, 0.051 mmol), H_4BTTB (13.6 mg, 0.024 mmol), N,N-dimethylformamide (DMF, 2.0 mL), EtOH (1.0 mL), H_2O (1.0 mL) and CF_3COOH (20 μL) was placed in a 10 mL glass vial and heated at 90 °C for 72 h. After it was cooled to room temperature at a rate of 5 °C h^{-1}, the purple needle crystals were collected.

Section 2. Structural analysis

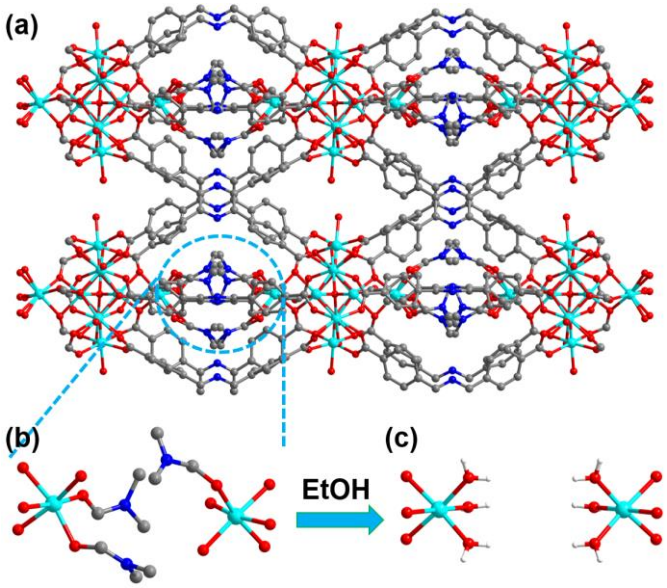

Fig. S1. The coordination mode between two adjacent clusters in **JNU-200** before solvent exchange.

Analyzing the spatial position of the distribution of 10 Co atoms in the Co-O cluster, as shown in the Fig. S2b and S2c†, there are six Co atoms as the six vertices of the hexagon, the included angle formed by every three adjacent Co atoms is 119.64°, and the Co-Co distances of two adjacent Co atoms are 3.388 Å and 3.272 Å, respectively. In addition, the remaining four Co atoms are symmetrically distributed on the vertical line of the hexagon. The Co-Co distances of the four cobalt

atoms on the vertical line are 2.913 Å, 2.490 Å, and 2.913 Å, respectively.

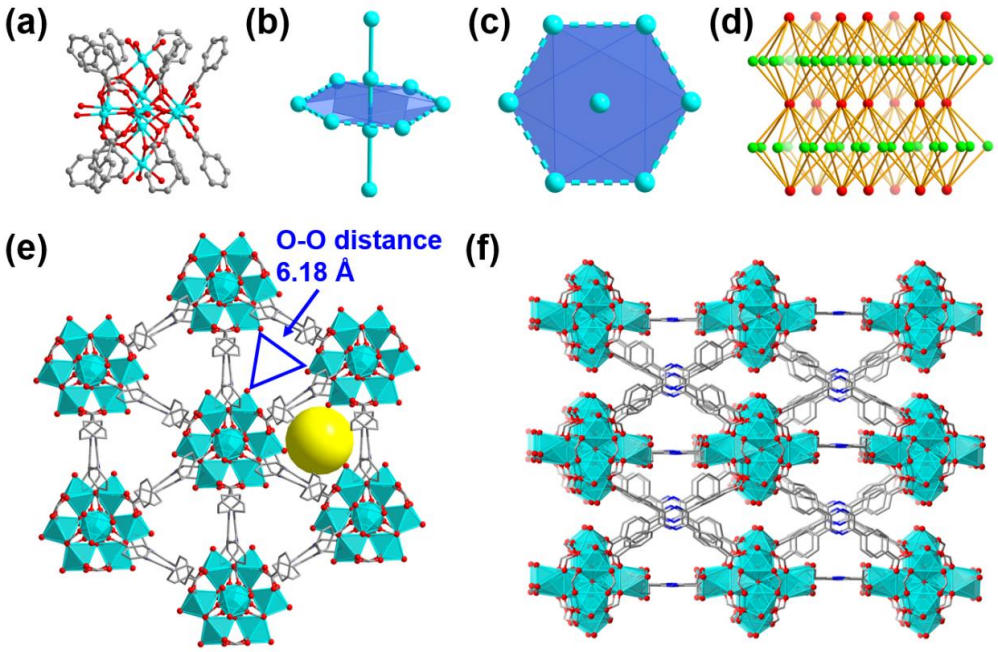

Fig. S2. (a) The coordination environment of $[Co_{10}(\mu_4\text{-}O)_3(CO_2)_{12}]$ SBUs. (b), (c) The relative position of Co atoms in a cobalt cluster. (d) Topological net for **JNU-200**. (e), (f) Ball-and-stick model of the **JNU-200** along *a* and *c* directions. (sky blue for Co, red for O, gray for C and blue for N, H atoms are not represented for the sake of clarity, yellow spheres highlight the triangular channels of **JNU-200**).

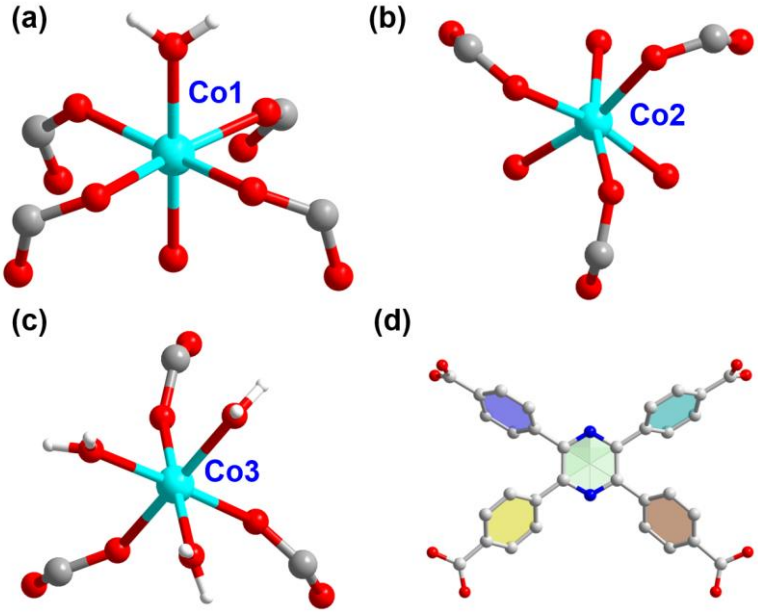

Fig. S3. Three different coordination modes of Co atom and organic ligand $BTTB^{4-}$. The $BTTB^{4-}$ linker is distorted with dihedral angles between the phenyl plane and the pyrazinyl plane (40.67°, 40.67°, 56.85°, and 56.85°; sky blue for Co, red for O, gray for C and blue for N, H atoms are not represented for the sake of clarity.)

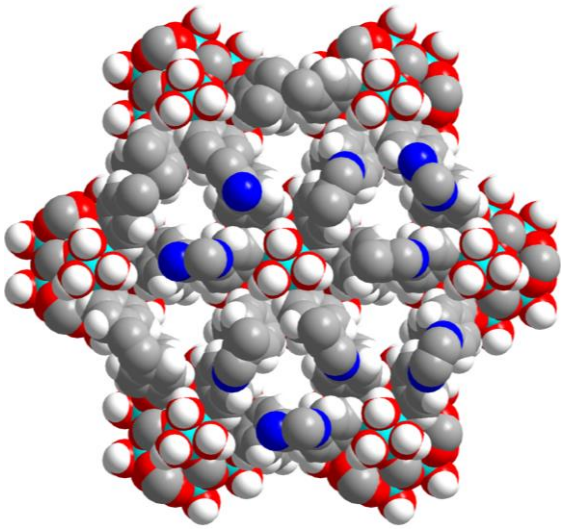

Fig. S4. Crystal structures of **JNU-200** in viewed along [001] direction in the space-filling model. (colour code: Co, turquoise; C, gray; N, blue; and O, red).

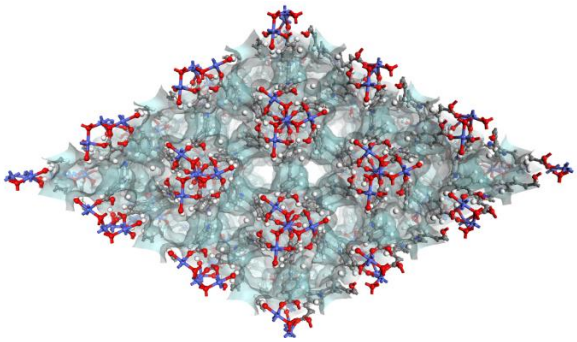

Fig. S5. Detailed inside view integrated with the Connolly surface (1D triangular channels (side length：6.0 Å), Color coding: H, white; C, gray; N, light blue; O, red; Co, blue).

Single-crystal X-ray diffraction analysis shows that **JNU-201** ($(Me_2NH_2)_4$ [$Co_7(\mu_2\text{-}O)_2$ $(BTTB)_4$ $(H_2O)_2$ $(DMF)_4$] $(H_2O)_4$ $(DMF)_{10}$) crystallizes in the monoclinic crystal system with a space group of *I*2/m. The 8-connected $Co_3(\mu_2\text{-}O)_2(H_2O)_2$ SBUs and $Co_2(\mu_2\text{-}O)(H_2O)_3$ are extended by the 4-connected tetracarboxylate linkers into a 2D framework (Fig. S6). Single-crystal X-ray diffraction analysis shows that **JNU-202** $(Me_2NH_2)_4$ [$Co_4(\mu_2\text{-}O)_2$ $(BTTB)_2$ H_2O $(HCO_2)_2(DMF)_2$] $(DMF)_4$ $(H_2O)_4$ crystallizes in the monoclinic crystal system with a space group of *P*2/c. The 4-connected $Co_2(H_2O)_2$EtOH SBUs are extended by the 4-connected tetracarboxylate linkers into a 3D framework (Fig. S7). Both **JNU-201** and **JNU-202** are constructed with low-nuclearity Co clusters. Therefore, the formation of high-nuclearity Co clusters could be hinged upon the pH of the reaction. It has been reported that pH is one of the factors affecting the formation of high-nuclearity clusters,[1] however, not in MOFs. The phase purity of bulk samples of **JNU-201** and **JNU-202** were confirmed

by comparison of their observed and simulated PXRD patterns (Fig. S8).

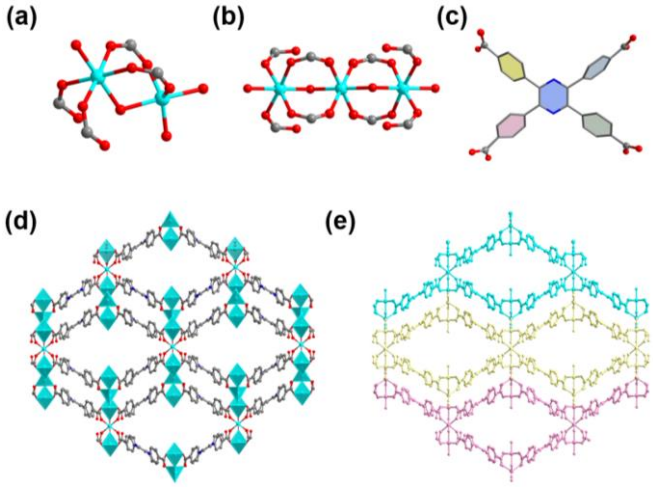

Fig. S6. (a) and (b) The Secondary building unit of **JNU-201**. (c) The configuration of the ligand in **JNU-201**. (d) Ball-and-stick model for **JNU-201** along *a* direction. (e) Two-dimensional layers stacking in **JNU-201**. The $BTTB^{4-}$ linker is distorted with dihedral angles between the phenyl plane and the pyrazinyl plane (44.44°, 45.48°, 51.32°, and 65.56°; sky blue for Co, red for O, gray for C and blue for N, H atoms are not represented for the sake of clarity.)

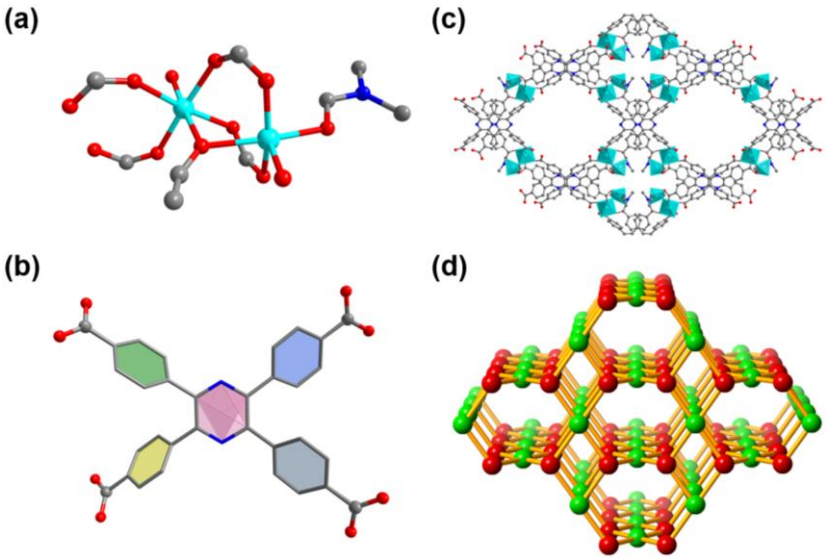

Fig. S7. (a) The Secondary building unit of **JNU-202**. (b)The configuration of the ligand in **JNU-202**. (c) Ball-and-stick model for **JNU-202** along *a* direction; The $BTTB^{4-}$ linker is distorted with dihedral angles between the phenyl plane and the pyrazinyl plane (34.66°, 34.66°, 52.07°, and 52.20°); (d) Topological net of **JNU-202** with **pts** topology. (sky blue for Co, red for O, gray for C, and blue for N, H atoms are not represented for the sake of clarity.)

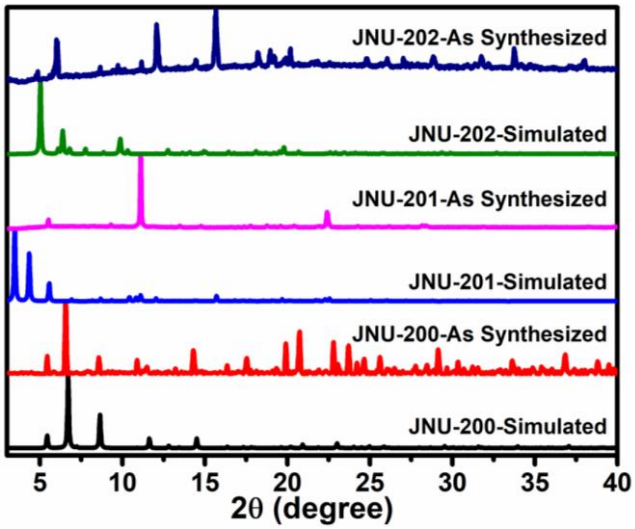

Fig. S8. PXRD patterns of **JNU-200**, **JNU-201**, and **JNU-202.**

Determination of the Crystal Structures

Single-crystal X-ray diffraction data of **JNU-200** (as-synthesized), **JNU-200** (ethanol exchanged), **JNU-200'**, **JNU-200"**. **JNU-200** and **JNU-200** were collected *via* an Oxford Cryo stream system on a XtaLAB PRO MM007-DW diffractometer system equipped with a RA-Micro7HF-MR-DW(Cu/Mo) X-ray generator and Pilatus3R-200K-A detector (Rigaku, Japan, Cu Kα, λ = 1.54178 Å) at 100(2) K. The numerical absorption corrections were applied using the program of ABSCOR. The structures were solved using direct methods, which yielded the positions of all non-hydrogen atoms, and they were refined anisotropically. Hydrogen atoms were placed in calculated positions with fixed isotropic thermal parameters and included in the structure factor calculations in the final stage of full-matrix least-squares refinement. All calculations were performed using the SHELXTL system of computer programs. The unit cell volume included a large region of disordered solvent which could not be modelled as discrete atomic sites. The treatment for the guest molecules in the cavities of all crystals involves the use of the SQUEEZE program of PLATON. Crystal data and structure refinement parameters are summarized in Tables S1. Topology information for the **JNU-200** was calculated by TOPOS 4.0.35.

Section 3. Crystallographic data

Table S1. Crystal data and structure refinement for **JNU-200** (as-synthesized), **JNU-200** (ethanol exchanged), **JNU-200'** and **JNU-200"**.

MOF	**JNU-200** (as-synthesized)	**JNU-200** (ethanol exchanged)	**JNU-200'**	**JNU-200"**
CCDC number	2059809	2059810	2059811	2059812
Empirical formula	$C_{34.63}H_{25.94}Co_{2.67}N_{2.88}O_{12}$	$C_{32.15}H_{22}Co_{2.64}N_2O_{12.13}$	$C_{96}H_{60}Co_{10}I_{7.13}N_6O_{33}$	$C_{96}H_{66}Co_9I_3N_6O_{36}$
Formula weight	831.86	786.00	3320.16	2790.56
Crystal system	hexagonal	hexagonal	hexagonal	hexagonal
Space group	$P\bar{6}2c$	$P\bar{6}2c$	$P\bar{6}2c$	$P\bar{6}2c$
a/ Å	15.20740(10)	15.0599(2)	15.3340(3)	15.1495(4)
b/ Å	15.20740(10)	15.0599(2)	15.3340(3)	15.1495(4)
c/ Å	32.4801(3)	32.6709(5)	32.2756(8)	32.4868(7)
V/ Å ^{3}	6505.16(10)	6417.1(2)	6573.8(2)	6457.1(3)
α/°	90	90	90	90
β/°	90	90	90	90
γ/°	120	120	120	120
Z	6	6	2	2
D_C /g cm $^{-3}$	1.274	1.220	1.678	1.435
μ /mm $^{-1}$	8.394	8.404	23.335	15.033
λ / Å	1.54184	1.54184	1.54184	1.54184
T/ K	100	100	100	100
Reflections collected	21573	28872	24941	20918
Independent reflections	4001 [R_{int} = 0.0839]	4573 [R_{int} = 0.0767]	4282 [R_{int} = 0.0529]	4395 [R_{int} = 0.0639]
Goodness-of-fit on F ^{2}	1.094	1.061	1.096	1.064
R_1[a], wR_2[b] [I > 2σ (I)]	R_1 = 0.1009, wR_2 = 0.2769	R_1 = 0.0960, wR_2 = 0.2616	R_1 = 0.1293, wR_2 = 0.3275	R_1 = 0.1232, wR_2 = 0.2878
R_1[a], wR_2[b] (all data)	R_1 = 0.1055, wR_2 = 0.2836	R_1 = 0.1006, wR_2 = 0.2667	R_1 = 0.1366, wR_2 = 0.3361	R_1 = 0.1362, wR_2 = 0.2975
Largest diff. peak and hole /e.Å $^{-3}$	1.44/-0.94	1.96/-1.19	2.64/-1.67	2.88/-1.29

[a] $R_1 = \Sigma||F_o| - |F_c|| / \Sigma|F_o|$

[b] $wR_2 = \{\Sigma[w (F_o^2 - F_c^2)^2]/[w (F_o^2)^2]\}$ 1/2 , $[F_o > 4\sigma (F_o)]$

Table S2. Crystal data and structure refinement for **JNU-201** and **JNU-202**.

MOF	**JNU-201**	**JNU-202**
CCDC number	2059813	2059814
Empirical formula	$C_{144}H_{130.66}Co_7N_{14}O_{48.67}$	$C_{74}H_{62}Co_4N_7O_{25}$
Formula weight	3248.43	1685.02
Crystal system	monoclinic	monoclinic
Space group	*I*2/m	*P*2/c
a/ Å	15.9042(2)	20.5687(3)
b/ Å	22.8367(5)	25.5953(3)
c/ Å	27.9925(5)	9.06771(10)
α/°	90	90
β/°	97.024(2)	97.3041(11)
γ/°	90	90
V/ Å ^{3}	10090.6(3)	4735.08(10)
Z	2	2
D_C /g cm $^{-3}$	1.069	1.182
μ /mm $^{-1}$	4.956	5.960
λ / Å	1.54184	1.54184
T/ K	100.01(15)	100.01(15)
Reflections collected	25393	26223
Independent reflections	10314	9608
Goodness-of-fit on F^2	1.027	1.041
R_1[a], wR_2[b] [$I > 2\sigma(I)$]	$R_1 = 0.1092$, $wR_2 = 0.2850$	$R_1 = 0.0991$, $wR_2 = 0.2822$
R_1[a], wR_2[b] (all data)	$R_1 = 0.1127$, $wR_2 = 0.2879$	$R_1 = 0.1083$, $wR_2 = 0.2947$
Largest diff. peak and hole /e.Å $^{-3}$	2.30/-0.93	1.71/-0.84

[a] $R_1 = \Sigma||F_o| - |F_c|| / \Sigma|F_o|$

[b] $wR_2 = \{\Sigma[w (F_o^2 - F_c^2)^2]/[w (F_o^2)^2]\}$ 1/2 , $[F_o > 4\sigma (F_o)]$

Section 4. General characterizations

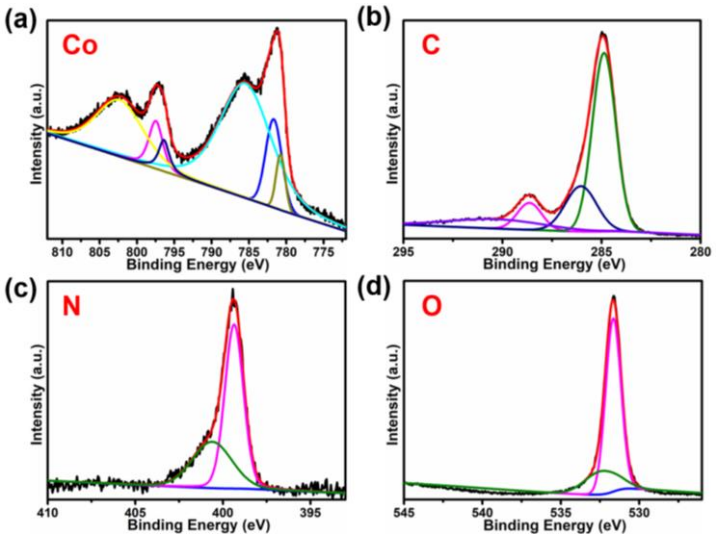

Fig. S9. High resolution XPS spectra of different elements in **JNU-200**.

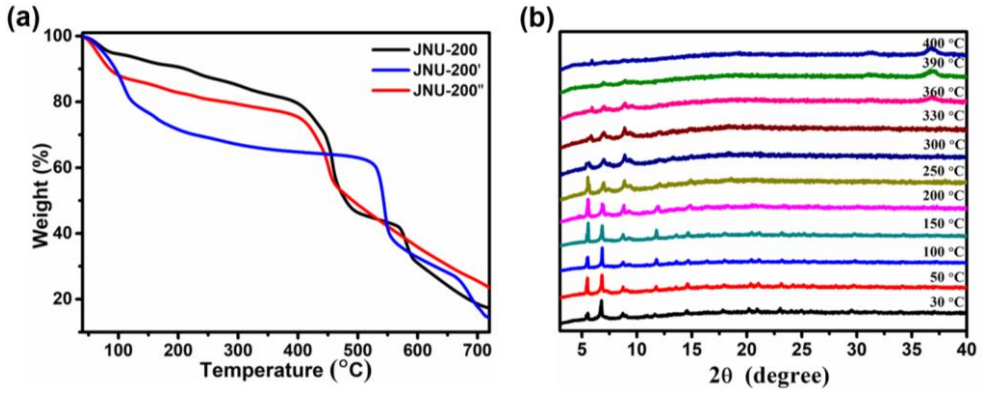

Fig. S10. (a) The TGA of **JNU-200**, **JNU-200'** and **JNU-200"**; (b) In-situ variable-temperature PXRD (VT-PXRD) patterns of **JNU-200** under ambient conditions.

Section 5. Iodine adsorption

The iodine adsorption capacity, Q (g/g), was calculated using equation (1)

$$Q = \frac{W_1 - W_0}{W_0} \qquad (1)$$

where W_1 and W_0 are the weights of **JNU-200** before and after iodine capture.[2]

The I_2 adsorption effi ciency (%) was obtained by the equation (2)

$$Adsorption\ efficiency\ (\%) = \left(\frac{C_0 - C_t}{C_0}\right) \times 100\% \qquad (2)$$

where C_0 and C_t (ppm) are the initial and time (t) I_2 concentrations, respectively.

The adsorption amount at equilibrium (Q_e) was obtained by equation (3)

$$Q_e = \left(\frac{C_0 - C_e}{m}\right) \times V \qquad (3)$$

where Q_e (mg g^{-1}) is the adsorbed amount at equilibrium; C_0 and C_e (ppm) are the initial and equilibrium I_2 concentrations; V (L) represents the volume of the I_2 solution, and m (g) is the mass of the MOF.

The adsorbed amount was calculated by equation (4)

$$Q_t = \left(\frac{C_0 - C_t}{m}\right) \times V \qquad (4)$$

where Q_t (mg g^{-1}) is the adsorption capacity at time t (min); C_0 is the initial concentration of I_2, C_t (ppm) is the concentration of I_2 at time t, V (L) is the volume of the solution, and m (g) is the mass of the MOF.

Fig. S11. The setup for iodine vapor adsorption.

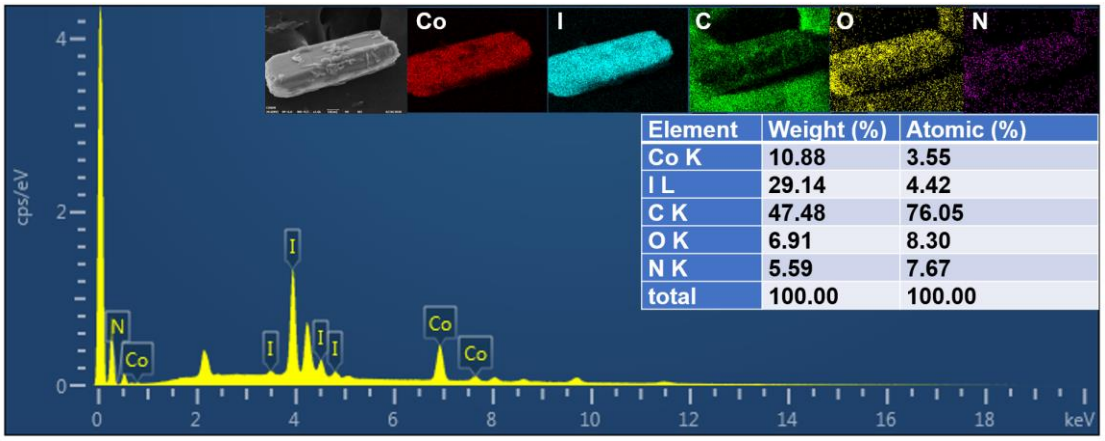

Fig. S12. SEM-EDS mapping and EDS spectra profiles of **JNU-200** after iodine vapor adsorption.

Table S3. A summary of some representative materials for the iodine capture.

MOFs	CCDC number	*P* calcg /cm^3	BET m^2/g	Iodine Uptake (g/g)	Iodine Uptake (wt.%)	Iodine Uptake g/cm^3	Test conditions	Ref
MOF-808	1002672	0.955	1930	2.18	218	2.08	80 □, I_2 (g)	2
HKUST-1	112954	0.958	1850	1.75	175	1.68	75 °C, I_2 (g)	3
NU-1000	1459134	/	2126	1.45	145	/	80 □, I_2 (g)	2

MOF-808-imidazole	/	/	1379	1.34	134	/	80 □, I_2 (g)	2
ZIF-8	602542	1.141	1630	1.25	125	1.43	77 I_2 (g)	4
MFM-300(In)	/	/	1050	1.16	116	/	80 °C, I_2 (g)	5
JNU-200	2059810	1.274	466	1.08	108	1.38	80 °C, I_2 (g)	This Work
Zn_3(DL-lac)$_2$(pybz)$_2$	745410	1.080	762.5	1	100	1.08	R.T. I_2 (l)	6
NU-1000-imidazole	/	/	1475	0.91	91	/	80 □, I_2 (g)	2
MOF-808-pyridine	/	/	1198	0.89	89	/	80 □, I_2 (g)	2
MOF-867	968930	0.756	2403	0.88	88	0.665	80 □, I_2 (g)	2
NU-1000-pyridine	/	/	1386	0.71	71	/	80 □, I_2 (g)	2
AlOC-26-NC	2042202	1.049	508	0.71	70.1	0.745	80°C, I_2 (g)	7
UiO-66	733458	/	1072	0.66	66	/	80 □, I_2 (g)	2
AlOC-28-NC	2042204	1.312	/	0.621	62.1	0.815	80°C, I_2 (g)	7
Micro-Cu_4I_4-MOF	1413643	1.297	641	0.13	12.5	0.169	R.T. I_2 (g)	8
{[(ZnI_2)$_3$(-TPT)$_2$]·5.5($C_6H_5NO_2$)}n	187830	2.065	/	0.59	37.2	1.22	80°C, I_2 (g)	9
UiO-67	/	/	2638	0.53	53	/	80 □, I_2 (g)	2
AlOC-27-NC	2042203	1.140	285	0.503	50.3	0.604	80°C, I_2 (g)	7
Th-SINAP-8	1960537	1.251	650	0.473	47.3	0.592	I_2 (l)	10
SBMOF-2	1039469	1.192	195	0.427	42.7	0.509	25 □, I_2 (g)	11
Th-SINAP-8	1960537	1.251	650	0.325	32.55	0.407	I_2 (g)	10
{[Co_3(BTC)$_2$(TIB)$_2$(H_2O)$_2$]·(H_2O)$_6$}n	977332	1.620	/	0.279	27.9	0.452	80°C, I_2 (g)	12
Th-SINAP-7	1960536	1.818	426	0.258	25.8	0.469	I_2 (l)	10
JNU-200	2059810	1.274	446	0.256	25.6	0.326	I_2 (l)	This Work
SBMOF-1	891520	1.624	145.15	0.226	22.6	0.367	25 □, I_2 (g)	11
Th-SINAP-7	1960536	1.818	426	0.107	10.7	0.195	I_2 (g)	10
Zn-BTC	1962948	0.987		0.2	20	0.197	I_2 (g)	13

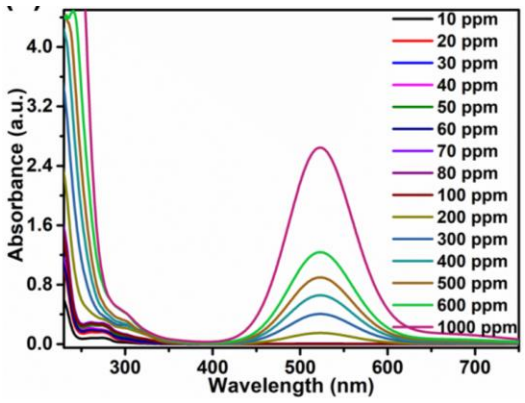

Fig. S13. UV-visible absorption spectra of hexane solutions (4 mL) of iodine at different concentrations after the addition of 4 mg **JNU-200** for 24 h.

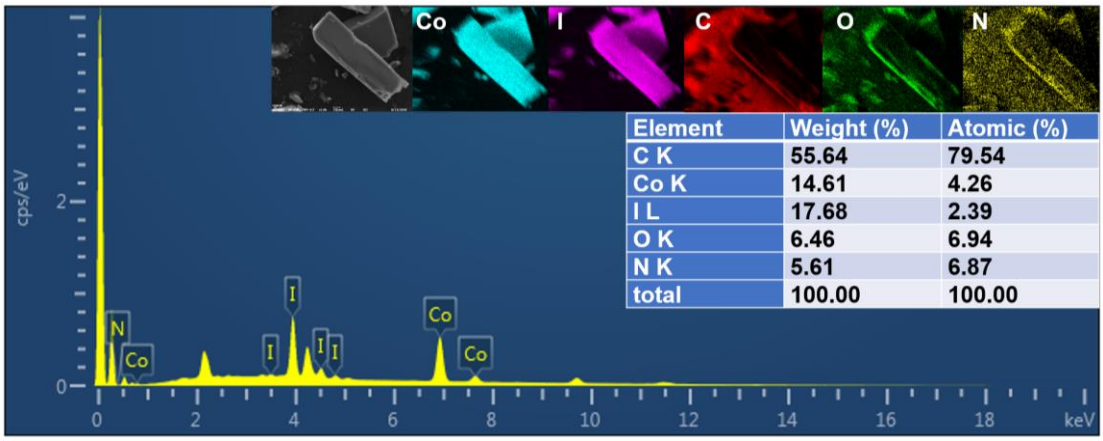

Element	Weight (%)	Atomic (%)
C K	55.64	79.54
Co K	14.61	4.26
I L	17.68	2.39
O K	6.46	6.94
N K	5.61	6.87
total	100.00	100.00

Fig. S14. SEM-EDS mapping and EDS spectra profiles of **JNU-200** after iodine absorption from a hexane solution.

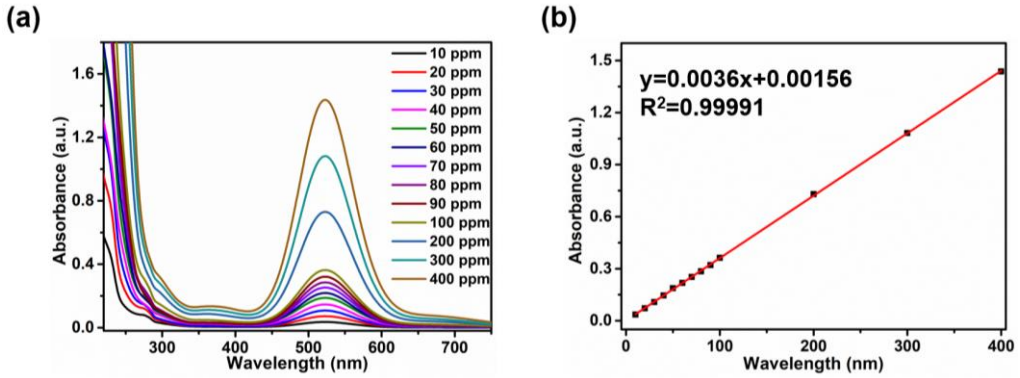

Fig. S15. UV-Vis absorption standard curve for iodine in hexane solution.

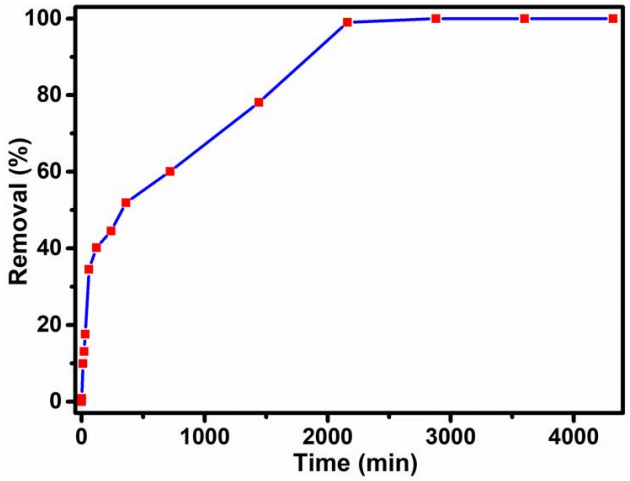

Fig. S16. Iodine adsorption kinetics of **JNU-200** in hexane solutions.

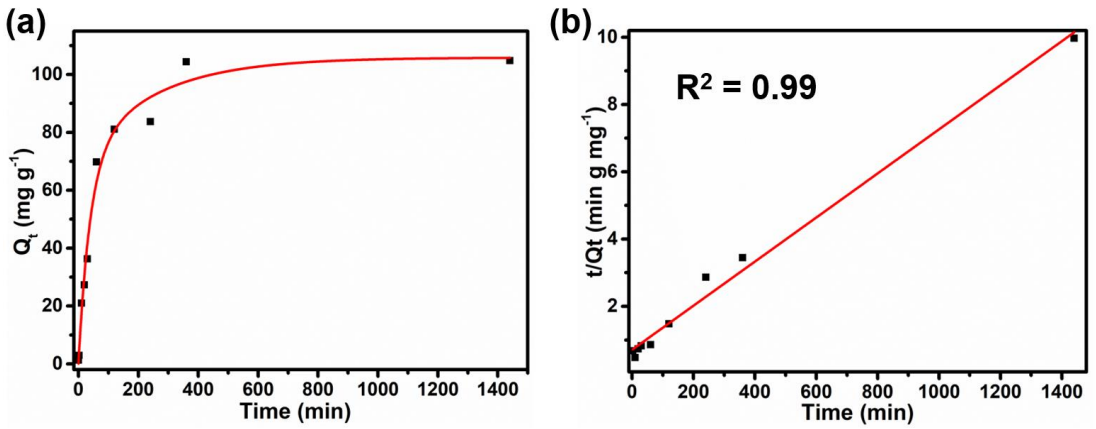

Fig. S17. (a) The change curve of Q_t with time; (b) Kinetic adsorption curves of the pseudo-second-order model for iodine adsorption of **JNU-200** in hexane solution.

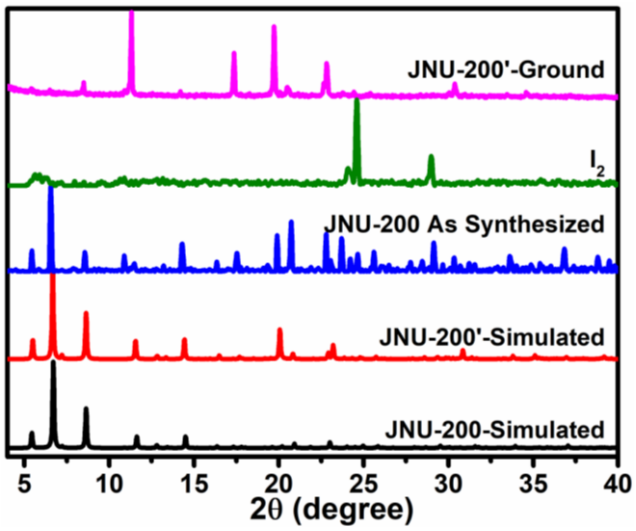

Fig. S18. PXRD patterns of **JNU-200** before and after iodine vapor adsorption.

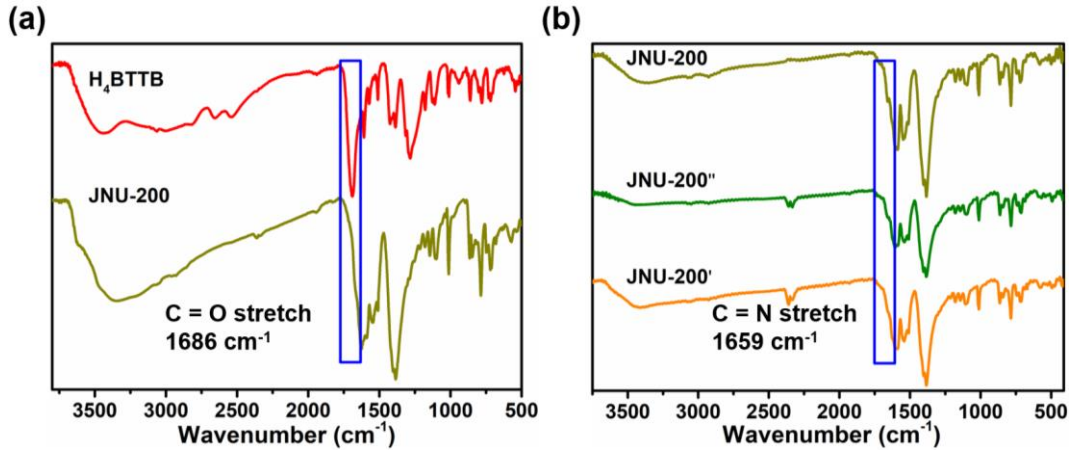

Fig. S19. FT-IR spectra of (a) H_4BTTB, **JNU-200** and (b) **JNU-200**, **JNU-200**'', **JNU-200**'.

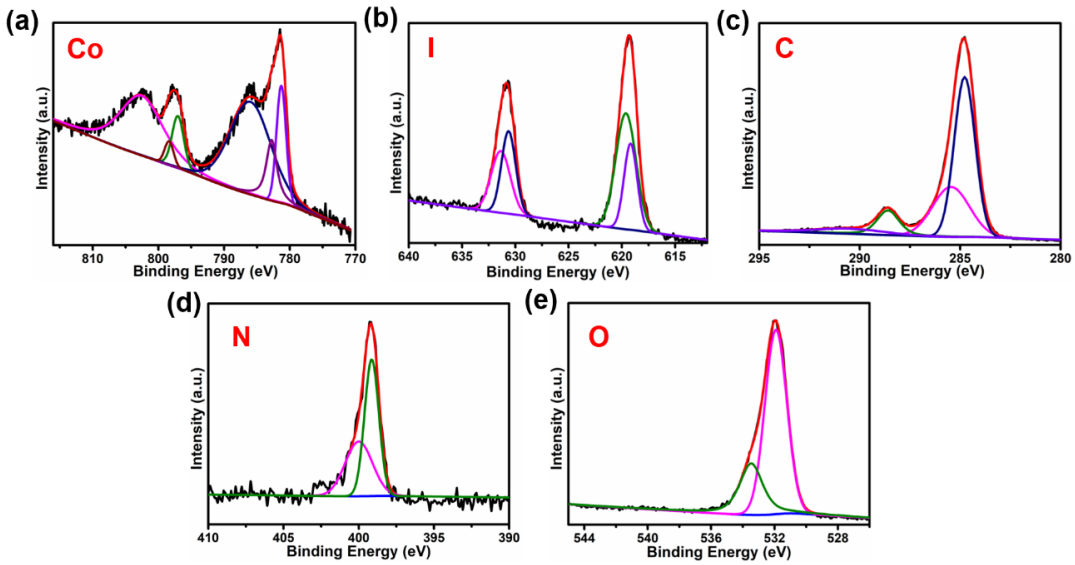

Fig. S20. High-resolution XPS spectra of different elements in **JNU-200'**.

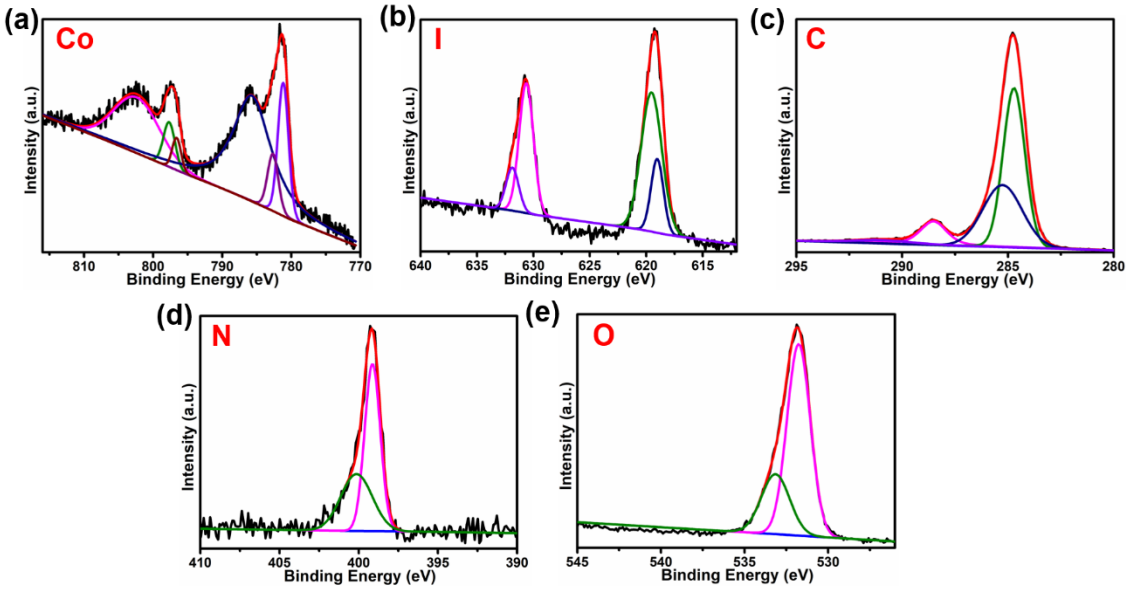

Fig. S21. High-resolution XPS spectra of different elements in **JNU-200"**.

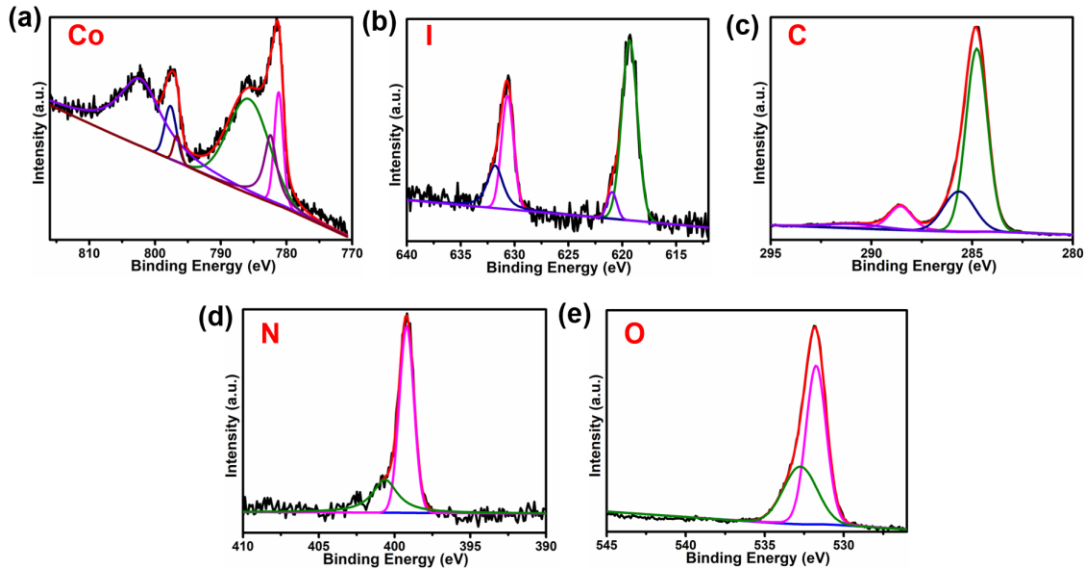

Fig. S22. High-resolution XPS spectra of different elements in **JNU-200'-EtOH**.

Table S4. XPS data for **JNU-200**, **JNU-200'**, **JNU-200"** and **JNU-200'-EtOH**.

	JNU-200	**JNU-200'**	**JNU-200"**	**JNU-200'-EtOH**
Co	802.29, 797.47 796.39, 785.46 781.68, 780.76,	802.55, 798.36, 797.04, 785.99, 782.77, 781.29	802.38, 797.68 796.60, 785.69 782.66, 781.17	802.28, 797.65 796.65, 785.71 782.42, 781.18
I	/	630.63, 619.63, 619.18, 631.37	630.63, 619.54, 619.03, 631.85	630.65, 620.95, 619.33, 631.81
C	290.28, 288.64, 284.88, 286.04	290.49, 288.59 284.78, 285.45	290.93, 288.52, 284.72, 285.26	290.90, 288.56 284.77, 285.66
N	399.36, 400.61	399.14, 400.00	399.13, 400.13	399.21, 400.63
O	531.65, 532.37	531.91, 533.47	531.75, 533.15	531.75, 532.74
Co^{3+}/Co^{2+} [a]	0.4325	1.5885	0.6816	0.64

[a] According to Co(III) $2p_{3/2}$ and Co(II) $2p_{3/2}$ peak areas.

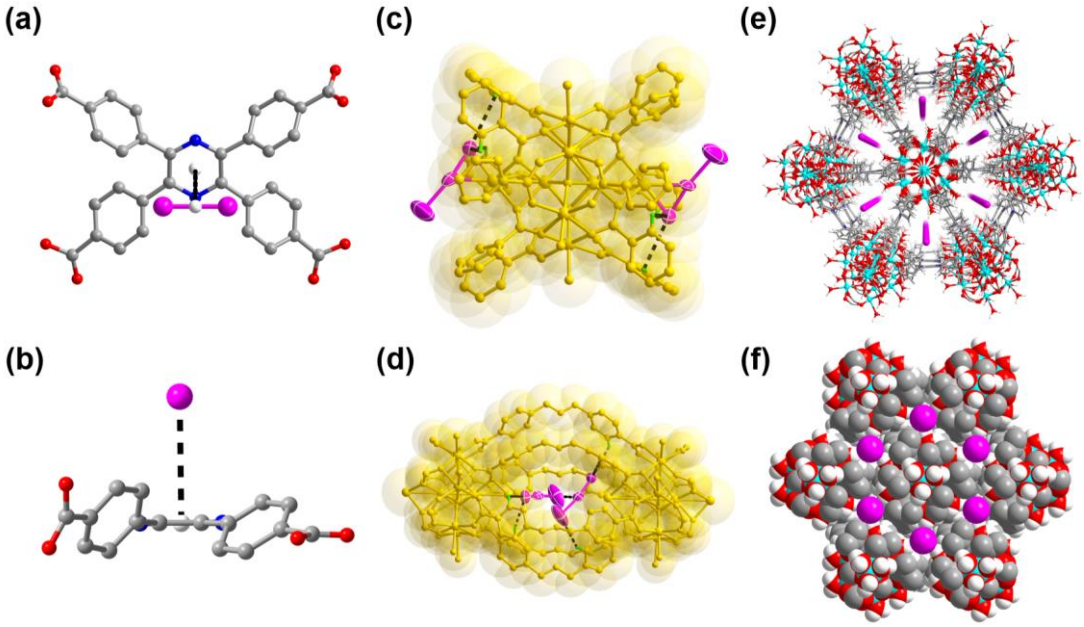

Fig. S23. Supramolecular interactions between iodine and framework (a) and (b) the distance between iodine and BTTB in the channel is 4.28 Å (I···π supramolecular interactions, dashed black line; white, dummy atom), (c) and (d) the I_3^- connected on the Co-O cluster, where the distance of C-H···I are 2.62 Å, 3.23 Å and 3.30 Å (dashed black lines), respectively; Crystal structures of **JNU-200**" in viewed along [001] direction in the (e) ball-and-stick and (f) space-filling model; sky blue for Co, red for O, gray for C, and blue for N.

Section 6. Histidine detection

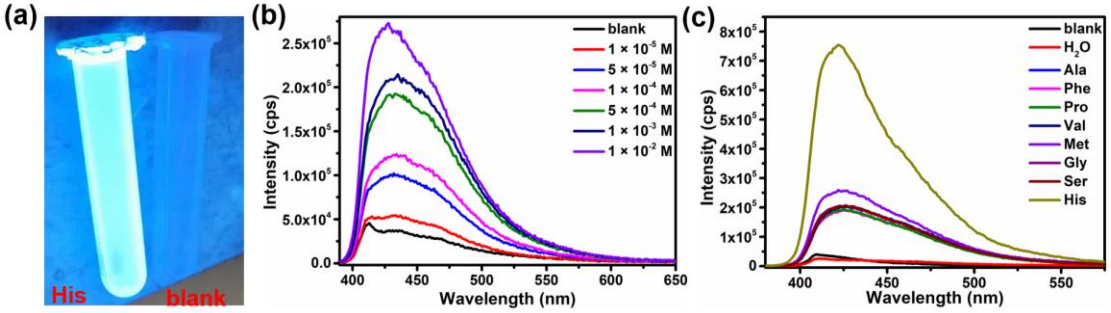

Fig. S24. (a) **JNU-200** suspension excited at 365 nm with or without His; (b) Concentration-dependent emission spectra of THF/H_2O suspensions of **JNU-200** (4 mg/100 mL) upon incremental addition of His under 365 nm excitation. (c) Luminescence emission spectra of THF/H_2O suspensions of **JNU-200** (4 mg/100 mL) in the presence of different amino acids (1.0 mM) under 365 nm excitation.

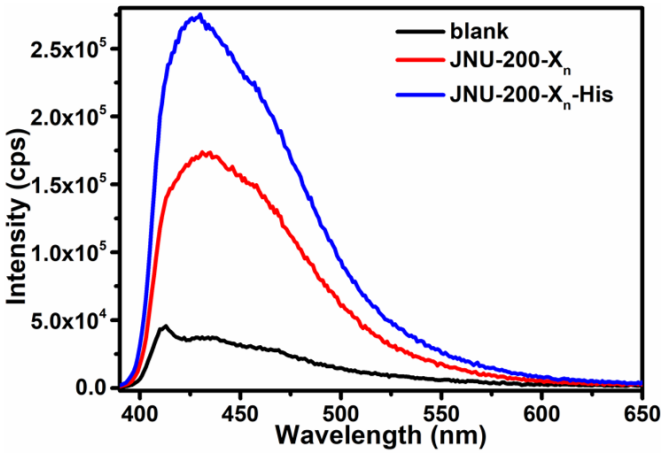

Fig. S25. Luminescence spectra of **JNU-200** suspensions upon the addition of His in the presence of seven amino acids (X = Ala, Phe, Pro, Val, Met, Gly, and Ser, 0.1 mM for each amino acid) under 365 nm excitation.

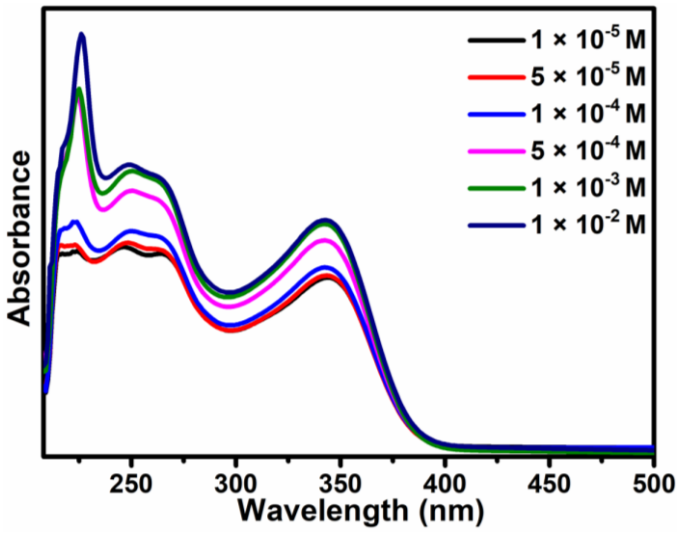

Fig. S26. Concentration-dependent UV-Visible absorption spectra of THF/H_2O suspensions of **JNU-200** at different concentrations under 365-nm excitation.

1. G. E. Kostakis, S. P. Perlepes, V. A. Blatov, D. M. Proserpio and A. K. Powell, *Coord. Chem. Rev.*, 2012, **256**, 1246-1278.
2. P. Chen, X. H. He, M. B. Pang, X. T. Dong, S. Zhao and W. Zhang, *ACS Appl. Mater. Interfaces*, 2020, **12**, 20429-20439.
3. D. F. Sava, K. W. Chapman, M. A. Rodriguez, J. A. Greathouse, P. S. Crozier, H. Zhao, P. J. Chupas and T. M. Nenoff, *Chem. Mater.*, 2013, **25**, 2591-2596.
4. D. F. Sava, M. A. Rodriguez, K. W. Chapman, P. J. Chupas, J. A. Greathouse, P. S. Crozier and T. M. Nenoff, *J. Am. Chem. Soc.*, 2011, **133**, 12398-12401.
5. X. Zhang, I. da Silva, H. G. W. Godfrey, S. K. Callear, S. A. Sapchenko, Y. Cheng, I. Vitorica-Yrezabal, M. D. Frogley, G. Cinque, C. C. Tang, C. Giacobbe, C. Dejoie, S. Rudic, A. J. Ramirez-Cuesta, M. A. Denecke, S. Yang and M. Schroder, *J. Am. Chem. Soc.*, 2017, **139**, 16289-16296.
6. Z. M. H, Q. X. Wang, Y. X. Tan, S. Hu, H. X. Zhao, L. S. Long and M. Kurmoo, *J. Am. Chem.*

Soc., 2010, **132**, 2561–2563

7. S. Yao, W. H. Fang, Y. Sun, S. T. Wang and J. Zhang, *J. Am. Chem. Soc.*, 2021, DOI: 10.1021/jacs.0c11778.
8. N. X. Zhu, C. W. Zhao, J. C. Wang, Y. A. Li and Y. B. Dong, *Chem Commun (Camb)*, 2016, **52**, 12702-12705.
9. G. Brunet, D. A. Safin, M. Z. Aghaji, K. Robeyns, I. Korobkov, T. K. Woo and M. Murugesu, *Chem. Sci.*, 2017, **8**, 3171-3177.
10. Z. J. Li, Z. H. Yue, Y. Ju, X. L. Wu, Y. M. Ren, S. F. Wang, Y. X. Li, Z. H. Zhang, X. F. Guo, J. Lin and J. A. Wang, *Inorg. Chem.*, 2020, **59**, 4435-4442.
11. D. Banerjee, X. Chen, S. S. Lobanov, A. M. Plonka, X. Chan, J. A. Daly, T. Kim, P. K. Thallapally and J. B. Parise, *ACS Appl. Mater. Interfaces*, 2018, **10**, 10622-10626.
12. Y. Rachuri, K. K. Bisht and E. Suresh, *Cryst. Growth Des.*, 2014, **14**, 3300-3308.
13. A. Sarkar, A. Adhikary, A. Mandal, T. Chakraborty and D. Das, *Cryst. Growth Des.*, 2020, **20**, 7833-7839.